This is the accepted manuscript made available via CHORUS. The article has been published as:

Gamow-Teller transitions to ^{93}Zr via the ^{93}Nb(t,^{3}He+γ) reaction at 115 MeV/u and its application to the stellar electron-capture rates

B. Gao, R. G. T. Zegers, J. C. Zamora, D. Bazin, B. A. Brown, P. Bender, H. L. Crawford, J. Engel, A. Falduto, A. Gade, P. Gastis, T. Ginter, C. J. Guess, S. Lipschutz, A. O. Macchiavelli, K. Miki, E. M. Ney, B. Longfellow, S. Noji, J. Pereira, J. Schmitt, C. Sullivan, R. Titus, and D. Weisshaar

Phys. Rev. C **101**, 014308 — Published 10 January 2020

DOI: 10.1103/PhysRevC.101.014308

Gamow-Teller transitions to ^{93}Zr via the ^{93}Nb(t,^{3}He+γ) reaction at 115 MeV/u and its application to the stellar electron-capture rates

B. Gao,[1,2,3,*] R. G. T. Zegers,[1,2,4] J. C. Zamora,[1,2,5] D. Bazin,[1,4] B. A. Brown,[1,2,4] P. Bender,[6] H. L. Crawford,[7] J. Engel,[8] A. Falduto,[9,2] A. Gade,[1,2,4] P. Gastis,[9,2] T. Ginter,[1] C. J. Guess,[10] S. Lipschutz,[1,2,4] A. O. Macchiavelli,[7] K. Miki,[11] E. M. Ney,[8] B. Longfellow,[1,4] S. Noji,[1,2] J. Pereira,[1,2] J. Schmitt,[1,2,4] C. Sullivan,[1,2,4] R. Titus,[1,2,4] and D. Weisshaar[1]

[1]*National Superconducting Cyclotron Laboratory, Michigan State University, East Lansing, Michigan 48824, USA*
[2]*Joint Institute for Nuclear Astrophysics - Center for the Evolution of the Elements, Michigan State University, East Lansing, MI 48824, USA*
[3]*Institute of Modern Physics, Chinese Academy of Sciences, Lanzhou 730000, China*
[4]*Department of Physics and Astronomy, Michigan State University, East Lansing, Michigan 48824, USA*
[5]*Instituto de Física, Universidade de São Paulo, 05508-090 São Paulo, Brazil*
[6]*Department of Physics, University of Massachusetss Lowell, Lowell, MA 01854, USA*
[7]*Lawrence Berkeley National Laboratory, Berkeley, CA 94720, USA*
[8]*Department of Physics and Astronomy, The University of North Carolina at Chapel Hill, Chapel Hill, NC 27599, USA*
[9]*Central Michigan University, Mount Pleasant, Michigan 48859, USA*
[10]*Department of Physics and Astronomy, Swarthmore College, Swarthmore, Pennsylvania 19081, USA*
[11]*Departament of Physics, Tohoku University, Sendai, Miyagi 980-8578, Japan*

(Dated: December 18, 2019)

Electron-capture reactions play important roles in the late evolution of core-collapse supernovae. The electron-capture rates used in astrophysical simulations rely on theoretical calculations which have to be tested against and guided by experimental data. We report on the measurement of the Gamow-Teller strength distribution of the odd-mass nucleus ^{93}Nb via the $(t,^3\mathrm{He}+\gamma)$ charge-exchange reaction at a beam energy of 115 MeV/u. The Gamow-Teller strength distributions were extracted up to an excitation energy in ^{93}Zr of 10 MeV. The results were compared with shell-model and quasiparticle random-phase approximation calculations. The theoretical calculations fail to describe the details of the strength distribution, but estimate reasonably well the integrated Gamow-Teller transition strength. Electron-capture rates derived from the measured and theoretical strength distributions match reasonably well, especially at the higher stellar densities of importance for deleptonization during the collapse of the stellar core, since the electron-capture Q-value is close to zero and the Fermi energy sufficiently high to ensure that the details of the strength distribution do not have a strong impact on the derived rates. At stellar densities in excess of 10^9 g/cm^3, the electron-capture rate based on a single-state approximation used in astrophysical simulations is slightly higher than the rates based on the data and the shell-model and QRPA calculations, likely due to the fact that the approximation includes temperature-dependent effects, which increase the rates. However, the difference is much smaller than observed in recent studies of nuclei with $Z < 40$ near $N = 50$, suggesting that the single-state approximation does not account for Pauli-blocking effects for nuclei with $Z < 40$ that are much stronger than for ^{93}Nb with $Z = 41$.

PACS numbers: 23.40.-s, 25.40.Kv, 26.50.+x, 27.60.+j

I. INTRODUCTION

The cataclysmic demise of massive stars in a core-collapse supernovae (CCSNe) are fascinating astrophysical phenomena. Understanding such phenomena is important for understanding the evolution of the Universe and the synthesis of elements [1, 2]. The occurrence rate of CCSNe in the Galaxy was estimated to be about two per century [3, 4]. Their signatures can be observed by detecting the neutrino and optical signals [1, 2, 5]. Gravitational waves emitted in the supernova explosion could provide further information about these events [6–9]. By combining the observational information with simulations, remaining open questions about the evolution, collapse, and explosion of CCSNe can be answered. It is important that the simulations have accurate physics inputs, including for relevant nuclear reactions.

Electron-capture (EC) reactions play an important role in CCSNe [1, 2, 10–16]. In the late stages of the evolution of massive stars, the gravitational forces on the iron core are balanced by the degeneracy pressure of electrons. When the mass of the core exceeds the Chandrasekhar limit of about 1.4 $M_\odot$, the electron degeneracy pressure can no longer support the core against the gravitational forces and the collapse ensues. However, even before the collapse, the density already becomes sufficiently high for the Fermi energy of the degenerate electrons to exceed the Q-value required for EC reactions to occur. Consequently, the electron fraction and degeneracy pressure are reduced due to the EC reactions,

* gaobsh@impcas.ac.cn; present address: Institute of Modern Physics, 509 Nanchang Rd., Lanzhou 730000, China.

accelerating the collapse. In addition, neutrinos emitted in the EC reaction escape and carry away energy and reduce the entropy inside the core. Therefore, the dynamical evolution of CCSNe is strongly affected by EC reactions and astrophysical simulations must include accurate estimates for EC rates.

Electron captures are dominated by allowed Gamow-Teller (GT) transitions in the β^+ direction. Here, the GT transition strength, B(GT), is defined such that the strength associated with the decay of the free neutron has B(GT)=3. Since a large number of elements are involved in the late stages of CCSNe and the rates are temperature and density dependent, one has to primarily rely on theoretical estimates for the GT transition-strength distributions from which the EC rates are derived. These theoretical calculations must be guided and benchmarked by comparison with experimental data.

During the late-stage evolution of CCSNe, electron-capture rates on medium-heavy, neutron-rich nuclei are most important [1, 8, 15, 17, 18]. Recently, several studies [19–22] have shown that electron captures on nuclei near $N = 50$ just above ^{78}Ni (hereafter we refer to this region as the high-sensitivity region) contribute most strongly to the deleptonization of the core. The EC rates in this region have previously been estimated by using a so-called single-state approximation [18, 23], in which the GT strength distribution is represented by a transition to a single state in the daughter nucleus. The excitation energy and strength of this transition were determined by fitting to electron-capture rates based on theoretical strength distributions that included temperature-dependent effects (transitions from excited states). However, as discussed in Ref. [20], this approximation does not account for the strong Pauli-blocking effects that occur in the high sensitivity region. These Pauli-blocking effects are caused by neutrons that occupy nuclear orbits that otherwise would be available for proton-hole, neutron-particle GT transitions in the β^+ direction. Therefore, it could lead to overestimates of the EC rates for neutron-rich nuclei in this region.

Experimental information on $B(\mathrm{GT}^+)$ distributions can be obtained by measuring the comparative half-life [log(ft)] of the β^+/EC-decaying nuclei. However, only the fraction of the $B(\mathrm{GT}^+)$ distribution within the Q-value window determined by the nuclear masses of the mother and daughter nuclei are accessible via decay measurements. During the core collapse, the EC reactions proceed primarily via neutron-rich nuclei, where the Q-value is negative and the β^+/EC decays are energetically not possible under terrestrial conditions. Charge-exchange (CE) reactions at intermediate energies ($\gtrsim 100$ MeV/u) provide an indirect way to measure the $B(\mathrm{GT}^+)$ distributions. The method is based on a well-established proportionality between the differential cross sections at small linear momentum transfer ($q \sim 0$) and $B(\mathrm{GT}^+)$ [24–27]. Since CE reactions are not limited by a Q-value window, they have become the preferred tool to probe $B(\mathrm{GT}^+)$ distributions up to high excitation energies, in particular for astrophysical purposes.

Here, we report on a ^{93}Nb(t, ^{3}He+γ) experiment aimed at extracting the GT strength distribution to ^{93}Zr. ^{93}Nb has $Z = 41$ and $N = 52$ and is on the proton-rich side of the above-mentioned high-sensitivity region. This work is part of a larger effort to study GT strength distributions in the $N = 50$ region, with two other experiments focusing on ^{88}Sr and ^{86}Kr [28, 29]. Pauli-blocking effects in ^{93}Nb are expected to be less severe than for these lighter nuclei with $Z \leq 40$, as the pf-shell and lower orbits cannot contain the 41 protons. The ground-state spin-parity of ^{93}Nb is $\frac{9}{2}^+$, associated with one proton occupying the $g_{9/2}$ orbit and GT transitions from the proton-$g_{9/2}$ orbit to the neutron-$g_{7/2}$ orbit are readily possible. In combination with measurements on nuclei with $Z \leq 40$ mentioned above, it is helpful to study ^{93}Nb in order to delineate Pauli-blocking effects in this region. Since previous measurements in this region of the chart of the nuclei have focused on even-even nuclei [30–33], it is also helpful to test the theoretical models in terms of reproducing the Gamow-Teller transition strength from an odd-mass nucleus, such as ^{93}Nb. Gamow-Teller transitions from ^{93}Nb populate final states with spin-parities of $7/2^+$, $9/2^+$, and $11/2^+$ and the theoretical calculations are more complex than for the 0^+ to 1^+ Gamow-Teller excitations from even-even nuclei.

II. EXPERIMENT

The experiment was performed at the Coupled Cyclotron Facility (CCF) at the National Superconducting Cyclotron Laboratory. A secondary triton beam was produced following the methods previously described in Ref. [34]. An ^{16}O primary beam with an intensity of 150 pnA and an energy of 150 MeV/u provided by the CCF impinged on a beryllium target with a thickness of 3525 mg/cm^2. The fragmentation products were purified in the A1900 fragment separator [35] by using a combination of magnetic rigidity and energy-loss ($B\rho$-ΔE-$B\rho$) selections. The aluminum wedge used at the intermediate image of the A1900 had a thickness of 195 mg/cm^2, which was sufficient for removing the vast majority of ^{6}He and ^{9}Li contaminants in the secondary rare-isotope cocktail beam. With these settings, about 3×10^6 tritons hit the ^{93}Nb target per second, with an energy of 115 MeV/u and a purity in excess of 99%. The ^{93}Nb foil was placed at the pivot point of the S800 spectrograph [36]. The beam line to the S800 spectrograph was operated in dispersion-matched mode [37], in which the momentum dispersion of the beam line up to the target matched that of the spectrograph from the target to the final focal plane. As a consequence, the momentum dispersion of the beam is cancelled in the transport of scattered particle through the spectrograph and the energy resolution that can be achieved in the (t,^{3}He) measurements is better than the energy spread in the triton beam.

The ^{93}Nb reaction target was 34-mg/cm^2 thick and

had a purity of 99.9%. A kapton foil ($C_{22}H_{10}N_2O_5$) with a thickness of 12.9 mg/cm^2 was also used to calibrate the triton beam intensity, as the differential cross section for the ^{12}C(t,^{3}He)^{12}B[1$^+$, ground state (g.s.)] was previously measured [26]. The ejectiles after the target were momentum analyzed by the S800 spectrograph set at a magnetic rigidity of 2.32 Tm. The ^{3}He ejectiles were detected with the focal-plane detector system of the S800 [38]. The two cathode-readout drift chambers (CRDCs) provided information on the hit positions and track angles of the ejectiles at the focal plane. A 5-mm thick plastic scintillation counter placed behind the CRDCs provided energy-loss (ΔE) and time-of-flight (TOF) information, the latter in combination with the radio-frequency (RF) signal of the CCF. By combining the ΔE and TOF information, scattered ^{3}He particles were cleanly identified.

The Gamma-Ray Energy Tracking In-beam Nuclear Array, GRETINA [39, 40], was placed around the reaction target to detect the deexcitation γ rays from the ^{93}Zr residual nucleus or its decay products after neutron and/or proton emission. The coincident measurement of the high-resolution γ rays and the ^{3}He ejectiles allows one to determine the GT transition strength of relatively weak transitions (with a strength of as low as B(GT)$\sim$ 0.01) to states at low excitation energy, which are difficult to identify in the singles data alone [41, 42]. For the experiment presented here, GRETINA consisted of thirty-two 36-fold segmented high-purity Ge detectors that provided about 1π solid-angle coverage. The photopeak detection efficiency was $\sim$4% for E_γ = 2 MeV.

III. DATA ANALYSIS AND RESULTS

A. Double-differential cross sections

For each event, the scattering angle and kinetic energy of the ^{3}He ejectile at the target position were reconstructed by using an inverse transfer matrix calculation, for which the angles and positions of the ejectiles measured in the focal plane served as inputs. The inverse transfer matrix was calculated by using the ion-optical code COSY Infinity [37]. The details about the reconstruction method are explained in Ref. [36].

The excitation energy of the ^{93}Zr residual nucleus was deduced by using a missing-mass calculation. To obtain absolute double-differential cross sections, $d^2\sigma/d\Omega dE$, the primary-beam intensity was continuously monitored by a Faraday bar located in the dipole magnet after the production target. The current readout of the Faraday bar was correlated to the triton beam intensity by using the known absolute cross section for the ^{12}C(t, ^{3}He)^{12}B(1$^+$,g.s.) reaction, for which the values have been accurately determined in a previous experiment [26]. The calibration runs were taken using the aforementioned kapton foil several times during the experiment. The systematic error induced by the beam intensity calibration was estimated to be 10%, which is the dominant source of systematic uncertainties in the absolute cross sections.

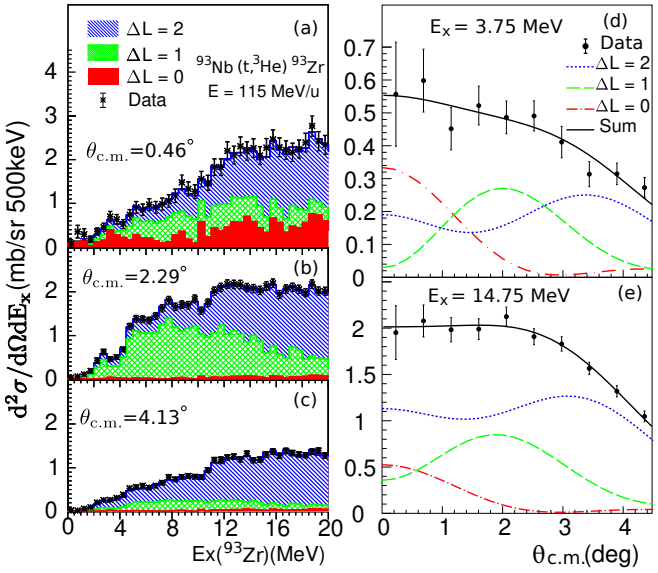

FIG. 1. (Color online) (Left) Double-differential cross section spectra for the ^{93}Nb(t,^{3}He) reaction at different scattering angles. The error bars represent the statistical uncertainties only. The histograms show contributions from excitations with different ΔL, obtained from the multipole-decomposition analysis (see Sec. III B). (Right) Representative angular distributions at E_x = 3.75 and 14.75 MeV and the results of multipole-decomposition analysis.

Some hydrogen or hydrogen-containing contaminants (water or oil) were absorbed on the ^{93}Nb foil and caused contamination in the ^{93}Nb(t,^{3}He) spectra due to ^{1}H(t,^{3}He) reactions. No γ rays associated with the decay of ^{12}B or daughters of ^{16}N (after particle decay) following ^{12}C,^{16}O(t,^{3}He) reactions could be identified and, even if present at very small levels, their contributions appear in the excitation energy spectrum of ^{93}Zr at excitation energies in excess of 10 MeV. By using clearly separated data for the ^{1}H(t,^{3}He) reaction from the calibrations with the kapton foil, this source of background was conveniently modelled and subtracted from the ^{93}Nb(t,^{3}He) spectra. Double-differential cross sections were determined up to an excitation energy of 20 MeV and for center-of-mass scattering angles of $\theta_{\rm c.m.} \lesssim 4.4°$ with an energy and angular resolution of 0.5 MeV and 1° (FWHM), respectively. The resulting excitation energy spectra for three scattering angles are shown in panels (a), (b) and (c) in Fig. 1.

B. Multipole-decomposition analysis

The double-differential cross sections obtained from the above procedure include contributions from excitations associated with different units of angular momentum transfer, ΔL. In order to extract the ΔL = 0 component, which is needed to determine the GT transi-

tion strength, a multipole-decomposition analysis (MDA) [43, 44] was performed. In the MDA, the angular distributions for each 0.5-MeV wide excitation-energy bin were fitted with a linear combination of angular distributions calculated in distorted-wave Born approximation (DWBA) with $\Delta L = 0$, 1 and 2. In the present work, the calculated angular distributions were obtained by using the double-folding DWBA code FOLD [45]. The optical-model potential parameters from the elastic scattering of the ^{3}He particles on the ^{90}Zr target at an incident energy of 443 MeV [46] were used for the outgoing channel. For the incoming channel, the real and imaginary depths of the Woods-Saxon potentials were scaled by a factor of 0.85 while keeping the other potential parameters (radii and diffusenesses) the same as the outgoing channel, following the procedure first used in Ref. [47]. For the ^{93}Nb-^{93}Zr target-residual system, the one-body transition densities (OBTDs) were determined using a normal-modes procedure [48] and the single-particle wave functions were generated by using a Woods-Saxon potential. For the triton and ^{3}He particles, the transition densities were taken from variational Monte Carlo calculations [49]. Although excitations with an angular momentum transfer of larger than 2 units can be populated, their contributions are expected to be small for the small linear angular-momentum transfers probed in the experiment. Moreover, their angular distributions at forward scattering angles are similar to the ones for the $\Delta L = 2$ excitations. Therefore, the results from the MDA for the $\Delta L = 2$ component essentially include contributions from excitations of higher angular-momentum transfer.

Two examples of the MDA, at excitation energies of 3.75 MeV and 14.75 MeV, are shown in panels (d) and (e) in Fig. 1. The results for all excitation-energy bins are included in the excitation-energy spectra in panels (a), (b) and (c) in Fig. 1. It is clear that $\Delta L = 0$ excitations contribute in the entire excitation-energy range covered in the experiment. This is very different from the results from the ^{88}Sr(t,^{3}He) reaction (taken with nearly the identical experimental setup) presented in Ref. [28], for which almost no monopole strength for excitation energies of up to 8 MeV was revealed. It is important to note that the excitation of the isovector spin giant monopole resonance (IVSGMR) starts to contribute significantly to the monopole excitations at excitation energies $E_x \gtrsim 10$ MeV [31, 50, 51]. Since the IVSGMR excitations are also associated with $\Delta L = 0$ and, therefore, have similar angular distribution as the GT excitations, their contributions cannot be separated from the GT transitions by the MDA used in this work. Therefore, we limit our studies of B(GT) up to E_x= 10 MeV, below which the $\Delta L = 0$ contributions are assumed to be due to GT excitations alone and contributions from the IVSGMR are negligible.

C. Extraction of GT strengths

After extracting the $\Delta L = 0$ component of the differential cross sections, the GT strengths were calculated by using the well-established proportionality between the differential cross sections at zero linear momentum transfer ($q = 0$ fm^{-1}) and B(GT) [24–26]:

$$\left(\frac{d\sigma}{d\Omega}\right)_{q=0} = \hat{\sigma} B(\mathrm{GT}), \tag{1}$$

where $\hat{\sigma}$ is the so-called unit cross section. The latter can be calibrated by using transitions for which the B(GT) values are known from β-decay data. In cases where such a calibration is not available, an empirical mass-dependent relationship, $\hat{\sigma} = 109A^{-0.65}$ mb/sr [25, 26] is usually used for (^{3}He,t) and (t,^{3}He) reactions at beam energies ranging from 115-140 MeV/u, where A is the mass number of the target nucleus. In the present work, $\hat{\sigma} = 109A^{-0.65}\ |_{A=93} = 5.73$ mb/sr was used. There are no transitions with known B(GT) available, as the ground state of ^{93}Zr has spin-parity of $\frac{5}{2}^+$ and the transition between ground states of ^{93}Zr and ^{93}Nb is of forbidden nature. The uncertainty in $\hat{\sigma}$ was estimated to be about 10% [26]. To obtain the differential cross section at $q = 0$ fm^{-1}, the extracted cross sections at $\theta = 0^\circ$ and finite Q-value from the MDA were extrapolated to $Q = 0$ MeV by using the DWBA calculations discussed above:

$$\left(\frac{d\sigma}{d\Omega}\right)_{q=0} = \left[\frac{\frac{d\sigma}{d\Omega}(Q=0,0^\circ)}{\frac{d\sigma}{d\Omega}(Q,0^\circ)}\right]_{\mathrm{DWBA}} \left[\frac{d\sigma}{d\Omega}(Q,0^\circ)\right]_{\mathrm{exp}}. \tag{2}$$

Here, the subscripts "DWBA" and "exp" represent the calculated and experimental values, respectively. After performing the procedure described above, the B(GT) values for each excitation energy bin were extracted by using Eq. (1). The results are shown in Fig. 2.

D. Analysis of coincident γ rays

The coincident γ rays emitted by the daughter nucleus ^{93}Zr can provide more detailed information on the transition strengths of individual low-lying states [41, 42]. Owing to the available phase space for EC in stellar environments, GT transitions to the lowest-lying states in the daughter nucleus contribute most strongly to the total electron-capture rates. With increasing stellar density, the Fermi energy increases and contributions from transitions to states at higher excitation energies increase. If the ground-state to ground-state electron-capture Q-value is small, as is the case for ^{93}Nb ($Q_{\mathrm{EC}} = -0.09$ MeV), the contribution from transitions to excited states is larger at lower stellar densities compared to nuclei for which the ground-state to ground-state electron-capture Q-value is high [29]. Since the present ^{93}Nb(t,^{3}He) singles data have an energy resolution of about 0.5 MeV

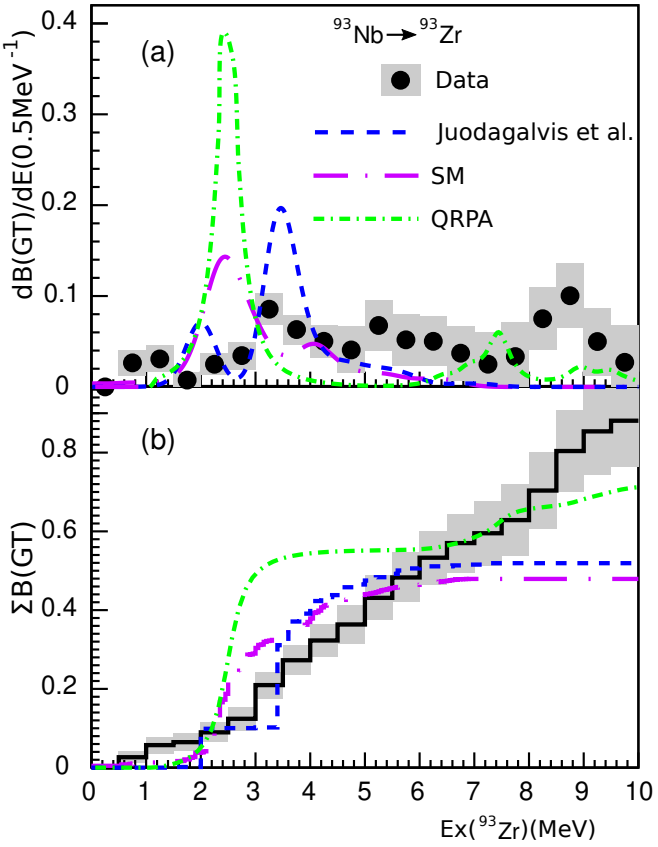

FIG. 2. (Color online) (a) $B(\mathrm{GT}^+)$ distributions for excitation from ^{93}Nb extracted from the experimental data (black dots). The shaded area represents the statistical errors only. The long dashed-dotted and short dashed-dotted lines represent the SM and QRPA calculations (see text in Sec. IV), respectively, carried out in the present work. The short-dashed curve represents SM calculations done by Juodagalvis et al. in Ref. [52]. The results from both sets of SM calculations have been smeared to account for the experimental resolution of 0.5 MeV(FWHM). For the QRPA calculation, the smearing was implicitly included in the calculation itself (see text). (b) The cumulative sum of the $B(\mathrm{GT}^+)$ distributions from the data and theoretical calculations as a function of excitation energy.

(FWHM) and GT transition strengths to low-lying states are small, it was not possible to identify individual low-lying transitions. However, the measurement of coincident γ rays by using GRETINA could be used to provide insight into the GT transition strength to the lowest-lying relevant state, at $E_x = 950$ keV [53].

A plot of the γ-ray energy E_γ as measured in GRETINA versus the excitation energy E_x of ^{93}Zr extracted from the $(t,^3\mathrm{He})$ data is shown in Fig. 3(a). The $E_x = E_\gamma$ line is drawn to guide the eye. The few data points appearing for $E_x < E_\gamma$ are an indication of the low background in the γ-coincident data. These background events are primarily due to reactions on hydrogen contaminant absorbed in the ^{93}Nb foil, as the $^1\mathrm{H}(t,^3\mathrm{He})$ reaction produces recoil neutrons that generate background when interacting in GRETINA or material surrounding the target.

As mentioned above, the first state in the daughter nucleus ^{93}Zr that can be populated by a GT transition is the $9/2^+$ state at $E_x = 950$ keV [53]. This state decays to the ground state with a branching ratio of 100%. No known other states with excitation energies below 2 MeV feed this $9/2^+$ level through multi-step γ-ray decays. Fig. 3(b) shows the γ-ray spectrum by gating on the excitation energy between 0.5 and 1.4 MeV. Three counts could be attributed to the decay of the 950-keV state to the ground state. By taking into account the detection efficiency of GRETINA, these counts can be converted into $B(\mathrm{GT})$ for the transition to the 950-keV state. The result is $0.031^{+0.029}_{-0.016}$. The errors of $+0.029$ and -0.016 correspond to the upper and lower limits of the 65% confidence level by assuming a Poisson distribution of the γ-ray counts. This result considers only statistical errors and is consistent with the strength of 0.053 ± 0.028 determined from the MDA procedure for the 0.5–1.5 MeV excitation-energy bins.

It is known that the proportionality of Eq. 1 is affected by the interference between the $\Delta L = 0$ and $\Delta L = 2$ amplitudes that both contribute to the $\Delta J = 1$ excitation. This interference is mediated via the tensor-τ component of the nucleon-nucleon interaction [54]. The interference induces systematic errors in the extraction of $B(\mathrm{GT})$ and errors are larger for very weak GT transitions. Based on the studies in Refs. [54, 55], the systematic error of $B(\mathrm{GT})$ of the 950-keV state induced by this interference was estimated to be 14%, corresponding to 0.004 in units of GT strength.

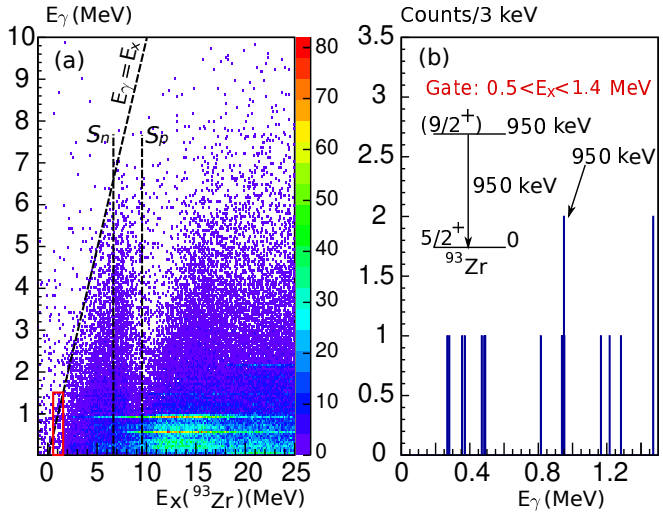

FIG. 3. (Color online) (a) Two-dimensional plot of the γ-ray energy E_γ versus excitation energy E_x. The $E_\gamma = E_x$ line and proton $(S_p)$and neutron (S_n) separation energies are indicated by dashed lines. (b) γ-ray energy spectrum gated on the excitation energy $0.5 < E_x < 1.4$ MeV which is indicated by the red box in (a). The inset shows a schematic decay diagram of the 950-keV state in ^{93}Zr.

A clear drop in the γ-ray yield and a lowering of the average γ-ray energy are observed around $E_x = 8$ MeV due to the opening of the neutron emission channel (neutron separation energy $S_n = 6.734$ MeV). Above that energy, γ lines associated with transitions in ^{92}Zr were detected in GRETINA, such as the 934- and 561-keV γ lines. At even higher excitation energies, other decay channels open. Decay by proton emission is possible above 9.595 MeV, but no significant signals from γ lines originating from ^{92}Y were observed, indicating that the decay by particle emission primarily occurs by neutron emission. It is somewhat surprising that the decay by neutron emission only becomes the dominant decay channel at 8 MeV, rather than immediately at $E_x = S_n$. To understand this phenomenon, the neutron and γ-ray emission probabilities were calculated as a function of E_x in the Hauser-Feshbach formalism [56] by using the nuclear evaporation code CASCADE [57, 58]. For excitation energies in ^{92}Zr and ^{93}Zr below 2.4 MeV and 1.7 MeV, respectively, known levels from Ref. [59] were inserted as inputs. At higher excitation energies, the back-shifted Fermi gas model [60] was used with parameters taken from Ref. [61]. Calculations were performed for initial total angular momentum states in ^{93}Zr of $\frac{1}{2}, \frac{3}{2}, ..., \frac{13}{2}$. As expected, the calculations showed that due to the angular momentum barrier, the decay by neutron emission is hindered for the decay from initial states with higher angular momentum, increasing the threshold for the decay. For states with low initial total angular momentum, the decay by neutron emission initiates right at the neutron separation energy. For states with an initial total angular momentum of $\frac{9}{2}$, the neutron emission channel opened between excitation energies of 7.5 and 8 MeV. As demonstrated by the MDA shown in Fig. 1, transitions with small relative angular momentum transfer from the ^{93}Nb ground state are favored, populating states in ^{93}Zr with total angular momenta close to $\frac{9}{2}$. Hence, it was concluded that the angular momentum barrier for neutron emission, in combination with the population of excited states in ^{93}Zr with relatively high total angular momentum, was the cause for the delayed opening of the neutron-emission channel.

IV. COMPARISON WITH THEORY

The extracted GT strength distributions up to $E_x = 10$ MeV were compared with different theoretical calculations as shown in Fig. 2. The first calculation was performed in the shell-model (SM) assuming a ^{78}Ni core, with a valence space of the ($0f_{5/2}$, $1p_{3/2}$, $1p_{1/2}$, $0g_{9/2}$) orbitals for protons and the ($0g_{7/2}$, $1d_{5/2}$, $1d_{3/2}$, $2s_{1/2}$, $0h_{11/2}$) orbitals for neutrons. The Hamiltonian was derived in the following manner. The proton-proton two-body matrix elements (TBME), as well as the proton single-particle energies, were based on the jj44pna interaction [62, 63]. The proton-neutron and neutron-neutron TBME were based on the renormalized G-matrix starting from the CD-Bonn interaction [64]. The neutron single-particle energies were determined from the experimental values of the observed single-particle states in ^{89}Sr. Due to the large dimensions involved in the calculation, the basis was truncated such that only up to 3 protons in the $0g_{9/2}$ orbital and no neutrons in the $0h_{11/2}$ orbital were allowed. Because the strengths are highly fragmented in the odd-A ^{93}Nb nucleus, 500 final states in ^{93}Zr for each of the spin-parities ($7/2^+$, $9/2^+$ and $11/2^+$) that can be accessed by GT transitions from the $9/2^+$ ground state in ^{93}Nb were calculated.

To account for the model-space truncations in our calculation, a mass-dependent hindrance factor h must be introduced [65] with which the calculated GT strengths should be renormalized:

$$B^*(\mathrm{GT}^+) = B(\mathrm{GT}^+)/h. \quad (3)$$

Here, $B(GT^+)$ is the GT strengths calculated using the above-mentioned model space, $B^*(\mathrm{GT}^+)$ is the renormalized GT strength. The hindrance factor h has two components [65]: $h = h_{high} \cdot h_{cp}$. The first component, h_{high}, is associated with configurations beyond the ($0g$, $1d$, $2s$) model space. It arises from the mixtures of two-particle two-hole states with unperturbed energies of $2\hbar\omega$ and higher in the oscillator basis. This has been extensively studied for the sd and pf shell nuclei [66, 67]. Here, we use the empirical value of $h_{high} = 1.81$ [67] for the ($0f$,$1p$) model space, since it is also consistent with the value observed for heavier nuclei [68].

The second component of the hindrance factor, h_{cp}, corresponds to the truncation from the ($0g$, $1d$, $2s$) space to the model space used in our calculation. In particular, the $\nu 0g_{9/2}$ orbital was assumed to be filled and the $\pi 0g_{7/2}$ orbital was assumed to be empty in our calculation. The hindrance factor h_{cp} accounts for the mixing between the $0g_{9/2}$ and $0g_{7/2}$ spin-orbit partners for the neutrons and for the protons due to core polarization that is missing in our model space. According to the calculations by Towner [65], h_{cp} depends strongly on the occupation number n of the $\pi 0g_{9/2}$ orbit. For the ^{93}Nb nucleus ($n = 1.78$ in our SM calculation), the value of $h_{cp} = 3.0$ was chosen based on the results for $n = 1$ and $n = 3$ in Ref. [65], that range from 2.2 to 3.7.

After taking into account the hindrance factors as discussed above, the calculated $B(\mathrm{GT}^+)$ strengths were compared with the experimental results in Fig. 2. Also shown in Fig. 2 are SM calculations from previous work done by Juodagalvis and Dean [52] where the authors systematically calculated the $B(\mathrm{GT}^+)$ distributions for the nuclei in the mass region $A = 90-97$. From Fig. 2(a) one can see that both sets of SM calculations do not reproduce the details of the strength distribution extracted from the data well. The SM calculations predict that most of the strength is concentrated in two peaks separated by slightly more than 1 MeV near $E_x = 3$ MeV. The experimental data exhibit a more fragmented strength distribution. As shown in Fig. 2(b), which displays the summed strength as a function of excitation energy, both

sets of SM calculations also miss strength at excitation energies above 6 MeV.

The $B(\mathrm{GT}^+)$ distribution was also calculated based on the quasiparticle random-phase approximation (QRPA) formalism. The QRPA result was obtained by applying a version of the axially-deformed Skyrme Finite Amplitude Method (FAM) [69, 70] extended to odd-A nuclei in the equal-filling approximation [71]. The method is, therefore, fully self-consistent for odd-A ground states computed in this approximation and a potentially attractive formalism to be used for a large group of nuclei of astrophysical interest. The latter is especially true since it is possible to include temperature-dependent effects in the future as well. The Skyrme functional and single-particle space are the same as those used in the global calculation of Ref. [72], which fixed a single set of parameters, including an effective axial-vector coupling constant g_A of 1.0, to compute the rates of even-even nuclei across the entire isotopic chart. The Hartree-Fock-Bogoliubov (HFB) ground state on which the QRPA calculation was carried out, was found to be slightly oblate, with a quadrupole deformation parameter $\beta_2 = -0.00658$. The location of the daughter ground-state energy was estimated from the HFB solution as the lowest one-quasiparticle transition energy. The QRPA calculation predicted a relatively strong state located at the same excitation energy of the SM calculation discussed above, with a minor amount of additional strength at excitation energies in excess of 6 MeV. Similar to both SM calculations presented above, the QRPA calculation has too much strength concentrated in a single or few states compared to the data. On the other hand, the integrated strength up to 10 MeV almost matches the experimental result.

V. DERIVED ELECTRON-CAPTURE RATES

Electron-capture rates were calculated on the basis of the experimentally extracted and theoretical strength distributions by using the following equation:

$$\lambda_{\mathrm{EC}}(T,\rho) = \ln 2 \sum_j \frac{f_j(T,\rho)}{ft_j}. \qquad (4)$$

Here, f_j is a calculable phase-space factor that depends on density and temperature and ft_j is the comparative half-life, which is derived from $B(\mathrm{GT})$. The index j runs over all the states in the daughter nucleus. Only transitions from the mother ground state are considered here. Since individual states in the daughter nucleus ^{93}Zr were not resolved in the experimental data, the index j represents excitation-energy bins up to an excitation energy of 10 MeV. However, for the EC rate to the 950-keV final state, the $B(\mathrm{GT})$ value extracted from the coincident γ-ray data was used, instead of the values extracted from the MDA procedure for the corresponding energy bin. The upper cut-off of 10 MeV in the excitation energy was not expected to have significant effects on the calculated

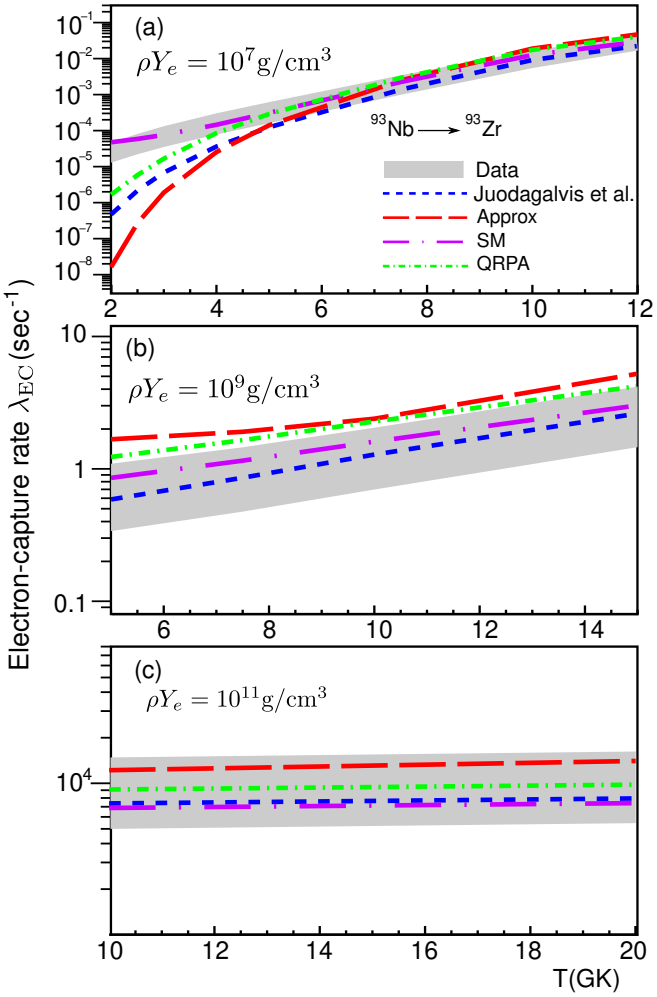

FIG. 4. (Color online) Calculated EC rates on ^{93}Nb as a function of temperature T(GK) at various stellar densities ρY_e(g/cm^3). The shaded area represents the results based on experimental data from the present work. The rates based on SM and QRPA calculations are represented by long dashed-dotted and short dashed-dotted lines, respectively. The rates based on SM calculations done by Juodagalvis et al. in Ref. [52] are represented by short-dashed lines. The rates calculated using the single-state approximation are also shown (long-dashed lines). The ΔE values (see text) used in the single-state approximation are 2.5 MeV in panel (a), 2.18 MeV (T = 5 GK), 2.46 MeV (T = 7.5 GK) and 2.74 MeV (T = 10 GK) in panel (b), 4.64 MeV (T = 10 GK) and 4.24 MeV (T = 20 GK) in panel (c), respectively.

EC rates since the theoretical calculations discussed in the previous section did not show significant amount of B(GT) above 10 MeV.

The calculations of EC rates follow the formalism of Refs. [73–76], implemented in a code previously used in Refs. [77, 78]. In addition to using Eq. (4), the EC rates were also evaluated using the single-state approximation mentioned in Sec. I. In this approximation, the EC rates

were calculated using the equation [18]:

$$\lambda = \frac{(\ln 2)B}{K}\left(\frac{T}{m_e c^2}\right)^5 [F_4(\eta) - 2\chi F_3(\eta) + \chi^2 F_2(\eta)], \quad (5)$$

where $\chi = (Q-\Delta E)/T$, $\eta = (\mu_e + Q - \Delta E)/T$, $K = 6146$ s and B represents a typical B(GT). The quantities F_k are the relativistic Fermi integrals of order k. The values of B and ΔE were obtained by fitting the microscopic calculations for nuclei near stability [18]. The value of $B = 4.6$ [18, 23] was used in the present work. The value of ΔE was determined following Ref. [23], rather than using a fixed value for all nuclei.

Fig. 4 shows the calculated EC rates as a function of temperature at three different densities multiplied with Y_e (the electron fraction): $\rho Y_e = 10^7$ g/cm^3, 10^9 g/cm^3, and 10^{11} g/cm^3 which cover typical stellar densities during the late stages of stellar evolution (from silicon burning to the onset of core collapse). At $\rho Y_e = 10^7$ g/cm^3 (Fig. 4(a)), the Fermi energy is just above 1 MeV, and the EC rate is very sensitive to the strength distribution at low excitation energies, especially when the stellar temperature is low and the Fermi surface sharp. Consequently, the theoretical models that best reproduce the low-lying strengths distribution observed in the experiment best reproduce the rates at low density and low temperature. In this case, the SM calculations performed as part of this work do the best, followed by the QRPA calculations and the SM calculations of Ref. [52]. The single-state approximation is less suitable for these low densities and Fermi energies, as it aims to mimic an average strength distribution by a single state that is placed at relatively high excitation energy. At higher temperature, the smearing of the Fermi surface becomes sufficiently large for transitions to a wider range of excitation energies to play a role, and the different calculations all are consistent with the data.

At $\rho Y_e = 10^9$ g/cm^3 (Fig. 4(b)), the Fermi energy is about 5 MeV. Consequently, the details of the strength distribution matter less than at the lower density and the EC rates only rise weakly with increasing temperature. However, the EC rate is not quite proportional to the integrated GT strength either, as the details of the strength distribution still bias the EC rates significantly. For example, the EC rate calculated based on the QRPA framework is quite close to that estimated based on the single-state approximation: the high strength associated with the latter is balanced by the placement of that strength at relatively high excitation energy compared to the QRPA calculation.

At $\rho Y_e = 10^{11}$ g/cm^3 (Fig. 4(c)), the Fermi energy is about 20 MeV, and the details of the strength distribution are nearly inconsequential, as is the smearing of the Fermi surface with increasing temperatures. These effects are enhanced by the fact that the ground-state to ground-state EC Q-value is close to zero for ^{93}Nb. For more neutron-rich systems, this is not the case and the very negative Q-values result in a stronger sensitivity to the details of the strength distribution, even at higher densities [29]. Here, the rate is nearly independent of temperature and more or less scales with the integrated GT strength. The single-state approximation produces a rate that is slightly higher than derived from the experimental data and the SM and QRPA calculations. This could (partially) be due to the fact that the single-state approximation was constructed to include the effects of transitions from excited states at high stellar temperatures. These effects are not included in the EC rate calculations using the GT strength distributions based on the experimental data, and the SM and QRPA calculations. However, we note that for the case of ^{93}Nb, the EC rate at high densities estimated using the single-state approximation is only slightly higher than the other theoretical estimates and the data and certainly much less than the factors of 10 to 100 observed for nuclei with $Z < 40$ near $N = 50$ [28, 29]. As Pauli-blocking effects are much stronger for those nuclei compared to ^{93}Nb, this result suggests that the single-state approximation is not suitable for estimating EC rates for nuclei where Pauli-blocking effects are very strong, such as in the high-sensitivity region [19, 20]. As this could strongly impact the simulations of the late evolution of CCSNe during its final stages prior to the explosion, further investigations including temperature-dependent effects are necessary.

VI. SUMMARY

Double-differential cross sections for the ^{93}Nb(t,^{3}He) charge-exchange reaction at 115 MeV/u were measured at the NSCL using the S800 spectrograph. The Gamow-Teller strength distribution was extracted by using a multipole-decomposition analysis and the proportionality between the differential cross section at vanishing momentum transfer for $\Delta L = 0$ excitations in charge-exchange reactions and the B(GT). The GRETINA γ-ray detector array was used to constrain the B(GT) of the lowest-lying state at 950 keV by detecting the associated γ rays. The experimental Gamow-Teller strength distribution was compared with SM and QRPA calculations. The theoretical calculations do not reproduce the details of the strength distribution: too much strength is concentrated in a few states compared to data, for which the Gamow-Teller strength is more distributed. The integrated Gamow-Teller strength up to 10 MeV extracted from the data is higher than predicted by the SM calculation, but close to the results from the QRPA calculations.

Derived electron-capture rates from the experimental and theoretical Gamow-Teller strength distributions show that the rates based on the theoretical models can reproduce the EC rates based on the data relatively well. This is due to the fact that the EC ground-state to ground-state Q-value for ^{93}Nb is small and the details of the strength distribution matter less than for nuclei for which this Q-value is much more negative. At the higher stellar densities, especially important for the strong deleptonization during the collapse of the core of

CCSNe, a single-state approximation used in astrophysical simulations predicts EC rates that are slightly higher than the EC rates based on the data, SM, and QRPA calculations. Since the parameters used in the approximation were derived by fitting the EC rates based on SM calculations where temperature-dependent effects were taken into account [18], the single-state approximation implicitly includes the temperature-dependent effects, which increases the EC rates. Such effects are presently missing from the other EC rate estimates, which could explain the difference of the estimated EC rates. However, the fact that the difference is quite small compared to factors of 10 to 100 observed for nuclei with $Z < 40$ near $N = 50$ suggests that the single-state approximation does not account properly for strong Pauli-blocking effects present in these lighter nuclei. These Pauli-blocking effects are not so strong for ^{93}Nb with $Z = 41$. Therefore, in combination with previous studies on ^{86}Kr [29] and ^{88}Sr [28], the results from the present work are important for better understanding and constraining electron-capture rates for astrophysical simulations, in particular those for CCSNe.

VII. ACKNOWLEDGMENTS

We thank the NSCL staff for their support during the preparations for and conducting of the experiment. This work was supported by the US National Science Foundation (NSF) under Cooperative Agreement PHY-156554 (NSCL), PHY-1430152 (JINA Center for the Evolution of the Elements), and PHY-1811855. GRETINA was funded by the US Department of Energy, in the Office of Nuclear Physics of the Office of Science. Operation of the array at NSCL was supported by DOE under Grants No. DE-SC0014537 (NSCL) and No. DE-AC02-05CH11231 (LBNL). B.G. thanks the support by the China Scholarship Council as part of the FRIB-CSC Fellowship. J.C.Z. thanks the support by Fundação de Amparo a Pesquisa do Estado de São Paulo (FAPESP) under Grant No. 2018/04965-4.

[1] H.-Th. Janka, K. Langanke, A. Marek, G. Martínez-Pinedo, and B. Müller, Phys. Rep. **442**, 38 (2007), the Hans Bethe Centennial Volume 1906-2006.
[2] H.-Th. Janka, F. Hanke, L. Hüdepohl, A. Marek, B. Müller, and M. Obergaulinger, Prog. Theor. Exp. Phys. **2012**, 01A309 (2012).
[3] R. Diehl, H. Halloin, K. Kretschmer, G. G. Lichti, V. Schönfelder, A. W. Strong, A. von Kienlin, W. Wang, P. Jean, J. Knödlseder, J.-P. Roques, G. Weidenspointner, S. Schanne, D. H. Hartmann, C. Winkler, and C. Wunderer, Nature **439**, 45 (2006).
[4] G. Bruno, W. Fulgione, A. Molinario, and C. Vigorito for the LVD Collaboration, J. Phys.: Conf. Ser. **888**, 012256 (2017).
[5] W. D. Arnett, Astrophys. J. **319**, 136 (1987).
[6] C. D. Ott, Class. and Quantum Grav. **26**, 063001 (2009).
[7] K. N. Yakunin, P. Marronetti, A. Mezzacappa, S. W. Bruenn, C.-T. Lee, M. A. Chertkow, W. R. Hix, J. M. Blondin, E. J. Lentz, O. E. B. Messer, and S. Yoshida, Class. and Quantum Grav. **27**, 194005 (2010).
[8] S. Richers, C. D. Ott, E. Abdikamalov, E. O'Connor, and C. Sullivan, Phys. Rev. D **95**, 063019 (2017).
[9] D. Radice, V. Morozova, A. Burrows, D. Vartanyan, and H. Nagakura, Astrophys. J. **876**, L9 (2019).
[10] C. L. Fryer, Astrophys. J. **522**, 413 (1999).
[11] A. Heger, C. L. Fryer, S. E. Woosley, N. Langer, and D. H. Hartmann, Astrophys. J. **591**, 288 (2003).
[12] A. Burrows, Rev. Mod. Phys. **85**, 245 (2013).
[13] K. Langanke and G. Martínez-Pinedo, Rev. Mod. Phys. **75**, 819 (2003).
[14] A. Heger, K. Langanke, G. Martínez-Pinedo, and S. E. Woosley, Phys. Rev. Lett. **86**, 1678 (2001).
[15] W. R. Hix, O. E. B. Messer, A. Mezzacappa, M. Liebendörfer, J. Sampaio, K. Langanke, D. J. Dean, and G. Martínez-Pinedo, Phys. Rev. Lett. **91**, 201102 (2003).
[16] A. Heger, S. E. Woosley, G. Martínez-Pinedo, and K. Langanke, Astrophys. J. **560**, 307 (2001).
[17] H. A. Bethe, G. E. Brown, J. Applegate, and J. M. Lattimer, Nucl. Phys. A **324**, 487 (1979).
[18] K. Langanke, G. Martínez-Pinedo, J. M. Sampaio, D. J. Dean, W. R. Hix, O. E. B. Messer, A. Mezzacappa, M. Liebendörfer, H.-Th. Janka, and M. Rampp, Phys. Rev. Lett. **90**, 241102 (2003).
[19] C. Sullivan, E. O'Connor, R. G. T. Zegers, T. Grubb, and S. M. Austin, Astrophys. J. **816**, 44 (2016).
[20] R. Titus, C. Sullivan, R. G. T. Zegers, B. A. Brown, and B. Gao, J. Phys. G: Nucl. Part. Phys. **45**, 014004 (2018).
[21] S. Furusawa, H. Nagakura, K. Sumiyoshi, C. Kato, and S. Yamada, Phys. Rev. C **95**, 025809 (2017).
[22] A. Pascal, S. Giraud, A. Fantina, F. Gulminelli, J. Novak, M. Oertel, and A. Raduta, "Impact of electron capture rates on nuclei far from stability on core-collapse supernovae," (2019), arXiv:1906.05114.
[23] Ad. R. Raduta, F. Gulminelli, and M. Oertel, Phys. Rev. C **95**, 025805 (2017).
[24] T. N. Taddeucci, C. A. Goulding, T. A. Carey, R. C. Byrd, C. D. Goodman, C. Gaarde, J. Larsen, D. Horen, J. Rapaport, and E. Sugarbaker, Nucl. Phys. A **469**, 125 (1987).
[25] R. G. T. Zegers, T. Adachi, H. Akimune, S. M. Austin, A. M. van den Berg, B. A. Brown, Y. Fujita, M. Fujiwara, S. Galès, C. J. Guess, M. N. Harakeh, H. Hashimoto, K. Hatanaka, R. Hayami, G. W. Hitt, M. E. Howard, M. Itoh, T. Kawabata, K. Kawase, M. Kinoshita, M. Matsubara, K. Nakanishi, S. Nakayama, S. Okumura, T. Ohta, Y. Sakemi, Y. Shimbara, Y. Shimizu, C. Scholl, C. Simenel, Y. Tameshige, A. Tamii, M. Uchida, T. Yamagata, and M. Yosoi, Phys. Rev. Lett. **99**, 202501 (2007).
[26] G. Perdikakis, R. G. T. Zegers, S. M. Austin, D. Bazin, C. Caesar, J. M. Deaven, A. Gade, D. Galaviz, G. F. Grinyer, C. J. Guess, C. Herlitzius, G. W. Hitt, M. E. Howard, R. Meharchand, S. Noji, H. Sakai, Y. Shimbara,

E. E. Smith, and C. Tur, Phys. Rev. C **83**, 054614 (2011).
[27] Y. Fujita, B. Rubio, and W. Gelletly, Prog. Part. Nucl. Phys. **66**, 549 (2011).
[28] J. C. Zamora, R. G. T. Zegers, S. M. Austin, D. Bazin, B. A. Brown, P. C. Bender, H. L. Crawford, J. Engel, A. Falduto, A. Gade, P. Gastis, B. Gao, T. Ginter, C. J. Guess, S. Lipschutz, B. Longfellow, A. O. Macchiavelli, K. Miki, E. Ney, S. Noji, J. Pereira, J. Schmitt, C. Sullivan, R. Titus, and D.Weisshaar, Phys. Rev. C **100**, 032801(R) (2019).
[29] R. Titus, E. M. Ney, R. G. T. Zegers, D. Bazin, J. Belarge, P. C. Bender, B. A. Brown, C. M. Campbell, B. Elman, J. Engel, A. Gade, B. Gao, E. Kwan, S. Lipschutz, B. Longfellow, E. Lunderberg, T. Mijatovic, S. Noji, J. Pereira, J. Schmitt, C. Sullivan, D. Weisshaar, and J. C. Zamora, Phys. Rev. C **100**, 045805 (2019).
[30] K. Miki, R. G. T. Zegers, S. M. Austin, D. Bazin, B. A. Brown, A. C. Dombos, R. K. Grzywacz, M. N. Harakeh, E. Kwan, S. N. Liddick, S. Lipschutz, E. Litvinova, M. Madurga, M. T. Mustonen, W. J. Ong, S. V. Paulauskas, G. Perdikakis, J. Pereira, W. A. Peters, C. Robin, M. Scott, A. Spyrou, C. Sullivan, and R. Titus, Phys. Lett. B **769**, 339 (2017).
[31] K. Miki, H. Sakai, T. Uesaka, H. Baba, C. L. Bai, G. P. A. Berg, N. Fukuda, D. Kameda, T. Kawabata, S. Kawase, T. Kubo, S. Michimasa, H. Miya, S. Noji, T. Ohnishi, S. Ota, A. Saito, Y. Sasamoto, H. Sagawa, M. Sasano, S. Shimoura, H. Takeda, H. Tokieda, K. Yako, Y. Yanagisawa, and R. G. T. Zegers, Phys. Rev. Lett. **108**, 262503 (2012).
[32] H. Condé, N. Olsson, E. Ramström, T. Rönnqvist, R. Zorro, J. Blomgren, A. Håkansson, G. Tibell, O. Jonsson, L. Nilsson, P.-U. Renberg, M. Österlund, W. Unkelbach, J. Wambach, S. Y. van der Werf, J. Ullmann, and S. A. Wender, Nucl. Phys. A **545**, 785 (1992).
[33] H. Dohmann, C. Bäumer, D. Frekers, E.-W. Grewe, M. N. Harakeh, S. Hollstein, H. Johansson, L. Popescu, S. Rakers, D. Savran, H. Simon, J. H. Thies, A. M. van den Berg, H. J. Wörtche, and A. Zilges, Phys. Rev. C **78**, 041602(R) (2008).
[34] G. W. Hitt, S. M. Austin, D. Bazin, A. L. Cole, J. Dietrich, A. Gade, M. E. Howard, S. D. Reitzner, B. M. Sherrill, C. Simenel, E. E. Smith, J. Stetson, A. Stolz, and R. G. T. Zegers, Nucl. Instrum. Methods A **566**, 264 (2006).
[35] D. J. Morrissey, B. M. Sherrill, M. Steiner, A. Stolz, and I. Wiedenhoever, Nucl. Instrum. Methods B **204**, 90 (2003).
[36] D. Bazin, J. A. Caggiano, B. M. Sherrill, J. Yurkon, and A. Zeller, Nucl. Instrum. Methods B **204**, 629 (2003).
[37] M. Berz, K. Joh, J. A. Nolen, B. M. Sherrill, and A. F. Zeller, Phys. Rev. C **47**, 537 (1993).
[38] J. Yurkon, D. Bazin, W. Benenson, D. J. Morrissey, B. M. Sherrill, D. Swan, and R. Swanson, Nucl. Instrum. Methods A **422**, 291 (1999).
[39] S. Paschalis, I. Y. Lee, A. O. Macchiavelli, C. M. Campbell, M. Cromaz, S. Gros, J. Pavan, J. Qian, R. M. Clark, H. L. Crawford, D. Doering, P. Fallon, C. Lionberger, T. Loew, M. Petri, T. Stezelberger, S. Zimmermann, D. C. Radford, K. Lagergren, D. Weisshaar, R. Winkler, T. Glasmacher, J. T. Anderson, and C. W. Beausang, Nucl. Instrum. Methods A **709**, 44 (2013).
[40] D. Weisshaar, D. Bazin, P. C. Bender, C. M. Campbell, F. Recchia, V. Bader, T. Baugher, J. Belarge, M. P. Carpenter, H. L. Crawford, M. Cromaz, B. Elman, P. Fallon, A. Forney, A. Gade, J. Harker, N. Kobayashi, C. Langer, T. Lauritsen, I. Y. Lee, A. Lemasson, B. Longfellow, E. Lunderberg, A. O. Macchiavelli, K. Miki, S. Momiyama, S. Noji, D. C. Radford, M. Scott, J. Sethi, S. R. Stroberg, C. Sullivan, R. Titus, A. Wiens, S. Williams, K. Wimmer, and S. Zhu, Nucl. Instrum. Methods A **847**, 187 (2017).
[41] S. Noji, R. G. T. Zegers, S. M. Austin, T. Baugher, D. Bazin, B. A. Brown, C. M. Campbell, A. L. Cole, H. J. Doster, A. Gade, C. J. Guess, S. Gupta, G. W. Hitt, C. Langer, S. Lipschutz, E. Lunderberg, R. Meharchand, Z. Meisel, G. Perdikakis, J. Pereira, F. Recchia, H. Schatz, M. Scott, S. R. Stroberg, C. Sullivan, L. Valdez, C. Walz, D. Weisshaar, S. J. Williams, and K. Wimmer, Phys. Rev. C **92**, 024312 (2015).
[42] S. Noji, R. G. T. Zegers, S. M. Austin, T. Baugher, D. Bazin, B. A. Brown, C. M. Campbell, A. L. Cole, H. J. Doster, A. Gade, C. J. Guess, S. Gupta, G. W. Hitt, C. Langer, S. Lipschutz, E. Lunderberg, R. Meharchand, Z. Meisel, G. Perdikakis, J. Pereira, F. Recchia, H. Schatz, M. Scott, S. R. Stroberg, C. Sullivan, L. Valdez, C. Walz, D. Weisshaar, S. J. Williams, and K. Wimmer, Phys. Rev. Lett. **112**, 252501 (2014).
[43] M. Ichimura, H. Sakai, and T. Wakasa, Prog. Part. Nucl. Phys. **56**, 446 (2006).
[44] B. Bonin, N. Alamanos, B. Berthier, G. Bruge, H. Faraggi, D. Legrand, J. C. Lugol, W. Mittig, L. Papineau, A. I. Yavin, D. K. Scott, M. Levine, J. Arvieux, L. Farvacque, and M. Buenerd, Nucl. Phys. A **430**, 349 (1984).
[45] J. Cook and J. Carr, Computer program FOLD/DWHI, Florida State University (unpublished); based on F. Petrovich and D. Stanley, Nucl. Phys. A **275**, 487 (1977); modified as described in J. Cook, K. W. Kemper, P. V. Drumm, L. K. Fifield, M. A. C. Hotchkis, T. R. Ophel, and C. L. Woods, Phys. Rev. C **30**, 1538 (1984); R. G. T. Zegers, S. Fracasso, and G. Colò (unpublished).
[46] J. Kamiya, K. Hatanaka, T. Adachi, K. Fujita, K. Hara, T. Kawabata, T. Noro, H. Sakaguchi, N. Sakamoto, Y. Sakemi, Y. Shimbara, Y. Shimizu, S. Terashima, M. Uchida, T. Wakasa, Y. Yasuda, H. P. Yoshida, and M. Yosoi, Phys. Rev. C **67**, 064612 (2003).
[47] S. Y. van der Werf, S. Brandenburg, P. Grasdijk, W. A. Sterrenburg, M. N. Harakeh, M. B. Greenfield, B. A. Brown, and M. Fujiwara, Nucl. Phys. A **496**, 305 (1989).
[48] M. A. Hofstee, S. Y. van der Werf, A. M. van den Berg, N. Blasi, J. A. Bordewijk, W. T. A. Borghols, R. De Leo, G. T. Emery, S. Fortier, S. Galès, M. N. Harakeh, P. den Heijer, C. W. de Jager, H. Langevin-Joliot, S. Micheletti, M. Morlet, M. Pignanelli, J. M. Schippers, H. de Vries, A. Willis, and A. van der Woude, Nucl. Phys. A **588**, 729 (1995).
[49] S. C. Pieper and R. B. Wiringa, Annu. Rev. Nucl. Part. Sci. **51**, 53 (2001); R. B. Wiringa, (private communication).
[50] I. Hamamoto and H. Sagawa, Phys. Rev. C **62**, 024319 (2000).
[51] C. J. Guess, T. Adachi, H. Akimune, A. Algora, S. M. Austin, D. Bazin, B. A. Brown, C. Caesar, J. M. Deaven, H. Ejiri, E. Estevez, D. Fang, A. Faessler, D. Frekers, H. Fujita, Y. Fujita, M. Fujiwara, G. F. Grinyer,

M. N. Harakeh, K. Hatanaka, C. Herlitzius, K. Hirota, G. W. Hitt, D. Ishikawa, H. Matsubara, R. Meharchand, F. Molina, H. Okamura, H. J. Ong, G. Perdikakis, V. Rodin, B. Rubio, Y. Shimbara, G. Süsoy, T. Suzuki, A. Tamii, J. H. Thies, C. Tur, N. Verhanovitz, M. Yosoi, J. Yurkon, R. G. T. Zegers, and J. Zenihiro, Phys. Rev. C **83**, 064318 (2011).

[52] A. Juodagalvis and D. J. Dean, Phys. Rev. C **72**, 024306 (2005).

[53] D. Pantelica, I. G. Stefan, N. Nica, M. G. Porquet, G. Duchêne, A. Astier, S. Courtin, I. Deloncle, F. Hoellinger, A. Bauchet, N. Buforn, L. Donadille, O. Dorvaux, J. Duprat, B. J. P. Gall, C. Gautherin, T. Kutsarova, S. Lalkovski, R. Lucas, M. Meyer, A. Minkova, A. Prévost, N. Redon, N. Schulz, H. Sergolle, O. Stézowski, T. Venkova, and A. Wilson, Phys. Rev. C **72**, 024304 (2005).

[54] R. G. T. Zegers, H. Akimune, S. M. Austin, D. Bazin, A. M. van den Berg, G. P. A. Berg, B. A. Brown, J. Brown, A. L. Cole, I. Daito, Y. Fujita, M. Fujiwara, S. Galès, M. N. Harakeh, H. Hashimoto, R. Hayami, G. W. Hitt, M. E. Howard, M. Itoh, J. Jänecke, T. Kawabata, K. Kawase, M. Kinoshita, T. Nakamura, K. Nakanishi, S. Nakayama, S. Okumura, W. A. Richter, D. A. Roberts, B. M. Sherrill, Y. Shimbara, M. Steiner, M. Uchida, H. Ueno, T. Yamagata, and M. Yosoi, Phys. Rev. C **74**, 024309 (2006).

[55] G. W. Hitt, R. G. T. Zegers, S. M. Austin, D. Bazin, A. Gade, D. Galaviz, C. J. Guess, M. Horoi, M. E. Howard, W. D. M. Rae, Y. Shimbara, E. E. Smith, and C. Tur, Phys. Rev. C **80**, 014313 (2009).

[56] W. Hauser and H. Feschbach, Phys. Rev. **87**, 366 (1952).

[57] F. Pühlhofer, Nucl. Phys. A **280**, 267 (1977).

[58] F. Pühlhofer, unpublished (1979), computer code CASCADE.

[59] C. M. Baglin, Nucl. Data Sheets **112**, 1163 (2011).

[60] E. Gadioli and L. Zetta, Phys. Rev. **167**, 1016 (1968).

[61] W. Dilg, W. Schantl, H. Vonach, and M. Uhl, Nucl. Phys. A **217**, 269 (1973).

[62] A. F. Lisetskiy, B. A. Brown, M. Horoi, and H. Grawe, Phys. Rev. C **70**, 044314 (2004).

[63] S. Mukhopadhyay, B. P. Crider, B. A. Brown, S. F. Ashley, A. Chakraborty, A. Kumar, M. T. McEllistrem, E. E. Peters, F. M. Prados-Estévez, and S. W. Yates, Phys. Rev. C **95**, 014327 (2017).

[64] I. Dillmann, K.-L. Kratz, A. Wöhr, O. Arndt, B. A. Brown, P. Hoff, M. Hjorth-Jensen, U. Köster, A. N. Ostrowski, B. Pfeiffer, D. Seweryniak, J. Shergur, and W. B. Walters (the ISOLDE Collaboration), Phys. Rev. Lett. **91**, 162503 (2003).

[65] I. S. Towner, Nucl. Phys. A **444**, 402 (1985).

[66] B. A. Brown and B. H. Wildenthal, At. Data Nucl. Data Tables **33**, 347 (1985).

[67] G. Martínez-Pinedo, A. Poves, E. Caurier, and A. P. Zuker, Phys. Rev. C **53**, R2602 (1996).

[68] C. Gaarde, in *Proc. Niels Bohr Centennial Conference on Nuclear Structure, Copenhagen*, edited by R. A. Broglia, G. B. Hagemann, and B. Herskind (North-Holland, Amsterdam, 1985) p. 449c.

[69] P. Avogadro and T. Nakatsukasa, Phys. Rev. C **84**, 014314 (2011).

[70] M. T. Mustonen, T. Shafer, Z. Zenginerler, and J. Engel, Phys. Rev. C **90**, 024308 (2014).

[71] T. Shafer, J. Engel, C. Fröhlich, G. C. McLaughlin, M. Mumpower, and R. Surman, Phys. Rev. C **94**, 055802 (2016).

[72] M. T. Mustonen and J. Engel, Phys. Rev. C **93**, 014304 (2016).

[73] G. M. Fuller, W. A. Fowler, and M. J. Newman, Astrophys. J. **293**, 1 (1985).

[74] G. M. Fuller, W. A. Fowler, and M. J. Newman, Astrophys. J. **252**, 715 (1982).

[75] G. M. Fuller, W. A. Fowler, and M. J. Newman, Astrophys. J. Suppl. Ser. **48**, 279 (1982).

[76] G. M. Fuller, W. A. Fowler, and M. J. Newman, Astrophys. J. Suppl. Ser. **42**, 447 (1980).

[77] A. L. Cole, T. S. Anderson, R. G. T. Zegers, S. M. Austin, B. A. Brown, L. Valdez, S. Gupta, G. W. Hitt, and O. Fawwaz, Phys. Rev. C **86**, 015809 (2012).

[78] S. Gupta, E. F. Brown, H. Schatz, P. Möller, and K.-L. Kratz, Astrophys. J. **662**, 1188 (2007).